OPA1 Controls Apoptotic Cristae Remodeling Independently from Mitochondrial Fusion

Christian Frezza,[1] Sara Cipolat,[1] Olga Martins de Brito,[1] Massimo Micaroni,[2] Galina V. Beznoussenko,[2] Tomasz Rudka,[3] Davide Bartoli,[1] Roman S. Polishuck,[2] Nika N. Danial,[4] Bart De Strooper,[3] and Luca Scorrano[1,*]
[1] Dulbecco-Telethon Institute, Venetian Institute of Molecular Medicine, Padova, Italy
[2] Department of Cell Biology and Oncology, Consorzio "Mario Negri Sud," Santa Maria Imbaro, Italy
[3] Neuronal Cell Biology and Gene Transfer Laboratory, Center for Human Genetics, Flanders Interuniversity Institute for Biotechnology (VIB4) and K.U. Leuven, Belgium
[4] Department of Cancer Biology, Dana-Farber Cancer Institute, Harvard Medical School, Boston, MA 02115, USA
*Contact: luca.scorrano@unipd.it
DOI 10.1016/j.cell.2006.06.025

SUMMARY

Mitochondria amplify activation of caspases during apoptosis by releasing cytochrome c and other cofactors. This is accompanied by fragmentation of the organelle and remodeling of the cristae. Here we provide evidence that Optic Atrophy 1 (OPA1), a profusion dynamin-related protein of the inner mitochondrial membrane mutated in dominant optic atrophy, protects from apoptosis by preventing cytochrome c release independently from mitochondrial fusion. OPA1 does not interfere with activation of the mitochondrial "gatekeepers" BAX and BAK, but it controls the shape of mitochondrial cristae, keeping their junctions tight during apoptosis. Tightness of cristae junctions correlates with oligomerization of two forms of OPA1, a soluble, intermembrane space and an integral inner membrane one. The proapoptotic BCL-2 family member BID, which widens cristae junctions, also disrupts OPA1 oligomers. Thus, OPA1 has genetically and molecularly distinct functions in mitochondrial fusion and in cristae remodeling during apoptosis.

INTRODUCTION

Mitochondria amplify apoptosis induced by several stimuli (Green and Kroemer, 2004). They release cytochrome c and other proapoptotic proteins activating a postmitochondrial pathway that culminates in cell demise (Wang, 2001). Proteins of the BCL-2 family control the release of cytochrome c from mitochondria required for the activation of effector caspases (Adams and Cory, 2001). The "BH3-only" proapoptotic members of the family transmit the different apoptotic signals to the multidomain members BAX and BAK that are required for cytochrome c release and mitochondrial dysfunction (Scorrano and Korsmeyer, 2003). In a widely accepted model, these proteins can form a channel for the efflux of cytochrome c across the outer mitochondrial membrane (Green and Kroemer, 2004). Additional pathways downstream of the BH3-only proteins ensure complete release of cytochrome c and mitochondrial dysfunction. They include fragmentation of the mitochondrial network and remodeling of the cristae characterized by fusion of individual cristae and opening of the cristae junctions (Frank et al., 2001; Scorrano et al., 2002).

Mitochondrial morphology is controlled by a growing family of "mitochondria-shaping" proteins (Griparic and van der Bliek, 2001). Mitofusin (MFN) -1 and -2 are dynamin-related proteins of the outer membrane (OM) essential for mitochondrial tethering and fusion (Santel and Fuller, 2001; Legros et al., 2002; Santel et al., 2003; Chen et al., 2003). MFN2 is presumed to have mostly a regulatory role (Ishihara et al., 2004), while MFN1 tethers two juxtaposed organelles (Koshiba et al., 2004) and cooperates with Optic Atrophy 1 (OPA1) in the fusion process (Cipolat et al., 2004). OPA1 is also a dynamin-related protein that resides in the inner mitochondrial membrane (IM). Dynamin-related protein 1 (DRP-1) is located in the cytoplasm but during fission translocates to mitochondria where it binds to hFis1, its adaptor in the OM (Smirnova et al., 2001; Yoon et al., 2003; James et al., 2003). It is presumed that DRP-1 can sever both membranes either directly or by recruiting other IM proteins.

A growing body of evidence suggests that mitochondria-shaping proteins participate in cell death. Dnm1p, the yeast ortholog of DRP-1, mediates mitochondrial fragmentation and apoptosis-like death in *S. cerevisiae* (Fannjiang et al., 2004). Blocking Drp-1 in *C. elegans* inhibits apoptotic mitochondrial fragmentation and results in the accumulation of supernumerary cells during development (Jagasia et al., 2005). Expression of a dominant negative mutant of DRP-1 or downregulation of hFis1 in

mammalian cells delays cytochrome c release and apoptosis (Frank et al., 2001; Lee et al., 2004). MFN1 and MFN2, alone or in combination, prevent death by some intrinsic stimuli (Sugioka et al., 2004; Neuspiel et al., 2005), consistent with early inhibition of MFN1-dependent fusion during apoptosis (Karbowski et al., 2004). Following several death stimuli, including the BH3-only proteins BID and BIK, mitochondria remodel their internal structure: individual cristae fuse and cristae junctions widen, allowing complete cytochrome c release (Scorrano et al., 2002; Germain et al., 2005). While the molecular details of mitochondrial fragmentation during apoptosis have been partially unraveled, little is known about the mechanisms controlling cristae remodeling, and we wished to further elucidate this process. OPA1 protects from apoptosis and is so far the only mitochondria-shaping protein associated with the IM (Olichon et al., 2003), making it a potential candidate to control cristae remodeling. Downregulation of OPA1 not only causes mitochondrial fragmentation but also alters the shape of the cristae (Olichon et al., 2003). Since cristae contain the bulk of cytochrome c, the regulation of this process could explain the known antiapoptotic effect of OPA1. Alternatively, OPA1 could act by counteracting mitochondrial fission (Lee et al., 2004). Here we genetically dissect the role of OPA1 in apoptosis and find that this can be separated from its role in mitochondrial fusion.

RESULTS

OPA1 Protects from Apoptosis by Preventing Cytochrome c Release and Mitochondrial Dysfunction

Expression of wild-type (wt) OPA1 protected mouse embryonic fibroblasts (MEFs) from death induced by apoptotic stimuli that activate the mitochondrial pathway like H_2O_2, etoposide, staurosporine, and truncated, active BID (tBID) (Wei et al., 2001; Scorrano et al., 2003) (Figures 1A–1D). OPA1 did not affect the extrinsic pathway of apoptosis recruited by TNFα since MEFs used in these experiments behave like type I cells not safeguarded by expression of BCL-2 (not shown). In type I cells, death receptors directly activate effector caspases, bypassing the mitochondrial amplificatory loop (Scaffidi et al., 1998). Mutation of a conserved Lys of the GTPase domain to Ala (OPA1[K301A]), or truncation of a part of the C-terminal coiled-coil domain (OPA1[R905*]) impair OPA1 pro-fusion activity (Cipolat et al., 2004). When these mutants were expressed at similar levels to wt OPA1 (data not shown and Cipolat et al., 2004), they failed to protect from all the stimuli tested (Figure 1). Thus, the GTPase and the C-terminal coiled-coil domains of OPA1 are required for protection from apoptosis.

OPA1 delayed release of cytochrome c following H_2O_2 (Figure 2A; quantification in Figure 2B), staurosporine (Figure S1B), etoposide, and tBID (not shown). Release of cytochrome c is accompanied by mitochondrial dysfunction and loss of mitochondrial membrane potential.
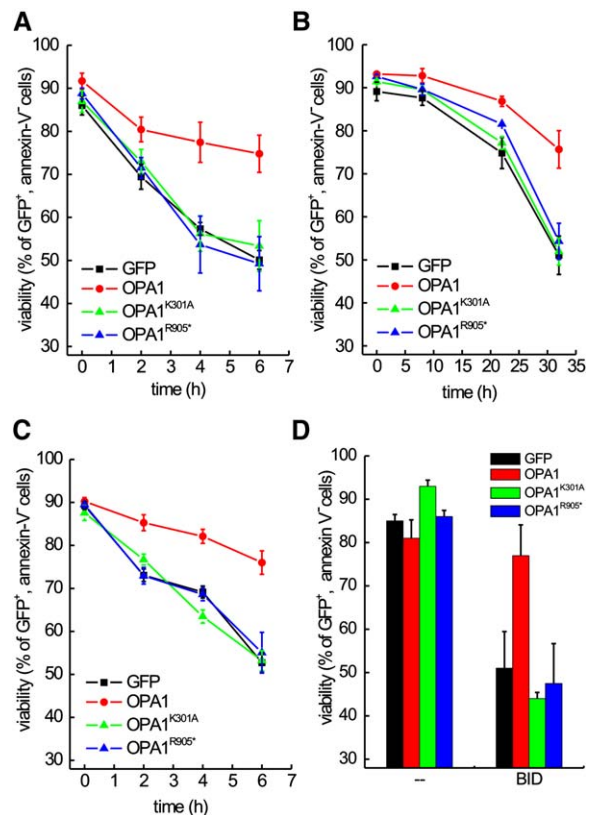
Figure 1. OPA1 Protects Against Apoptosis by Intrinsic Stimuli

wt MEFs were cotransfected with GFP and the indicated plasmids and after 24 hr treated with 1 mM H_2O_2 (A) (mean ± SEM of 12 independent experiments), 2 μM etoposide (B) (mean ± SEM of 12 independent experiments), or 2 μM staurosporine (C) (mean ± SEM of 12 independent experiments) for the indicated times. In (D) cells were cotransfected with GFP and pcDNA3.1 or with pcDNA3.1-tBID and after 24 hr viability was determined. Data represent average ± SEM of 7–12 independent experiments.

We followed in real time changes in the mitochondrial fluorescence of the potentiometric probe tetramethylrhodamine methylester (TMRM). OPA1 prevented depolarization induced by H_2O_2 (Figures 2C and 2D). Conversely, OPA1[K301A] had no such protective effects on cytochrome c release and mitochondria depolarization (Figures 2C and 2D). These results indicate that functional OPA1 decreases release of cytochrome c and loss of mitochondrial membrane potential during apoptosis.

OPA1 Does Not Require Mitofusins to Protect from Apoptosis

OPA1 requires *Mfn1* for its profusion activity (Cipolat et al., 2004). To check whether OPA1 protects against apoptosis by promoting fusion, we expressed OPA1 in MEFs lacking *Mfn1*. OPA1 protected *Mfn1*^{−/−} cells from apoptosis induced by all the intrinsic stimuli tested to an extent similar to that observed in wt cells (Figures 3A–3C). Since residual mitochondrial fusion is still observed in *Mfn1*^{−/−} MEFs, we
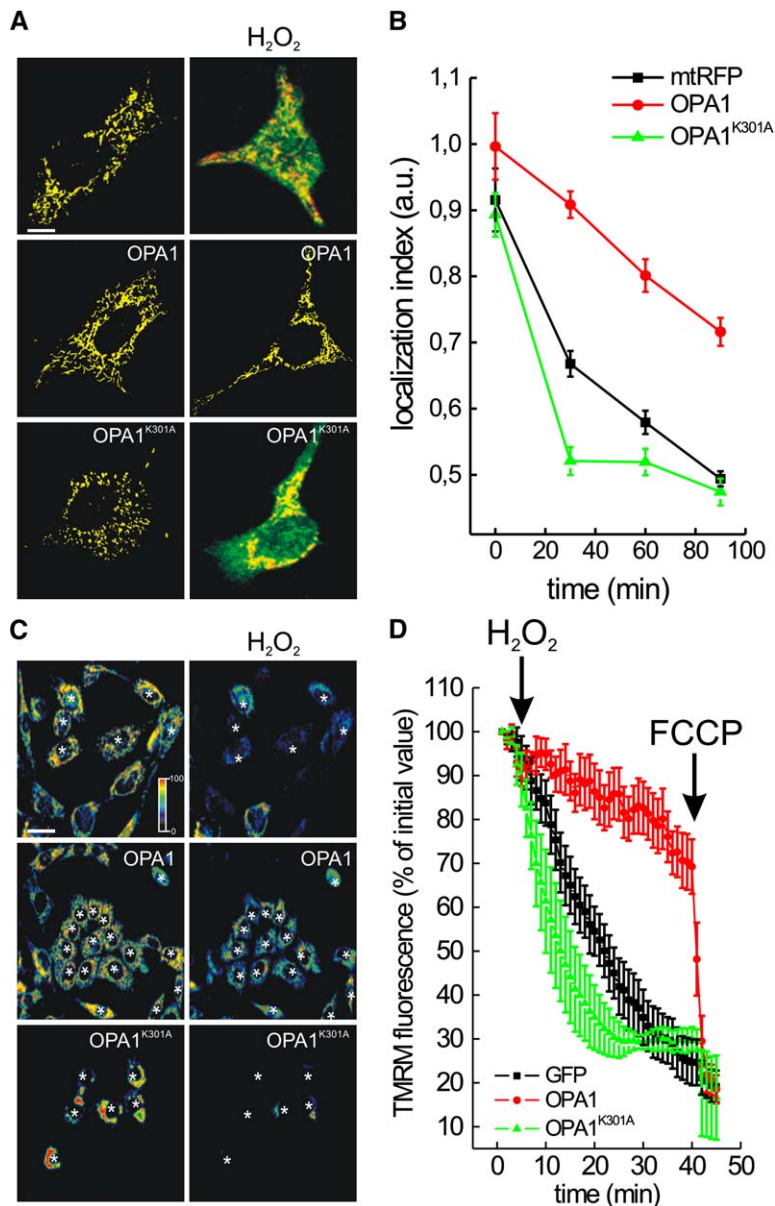
Figure 2. OPA1 Delays Release of Cytochrome c and Mitochondrial Dysfunction during Apoptosis

(A) Representative images of subcellular cytochrome c distribution. wt MEFs were cotransfected with mtRFP (red), and the indicated plasmids were left untreated or treated for 30 min with 1 mM H₂O₂, fixed and immunostained for cytochrome c (green). Bar, 15 μm.

(B) Localization index of cytochrome c. Experiments were performed as in (A), but cells were fixed at the indicated times. Data represent mean ± SEM of five independent experiments.

(C) Pseudocolor-coded images of TMRM fluorescence in wt MEFs cotransfected with GFP and the indicated plasmids. Left images represent the initial frame of the real-time sequence, while right ones were acquired at time = 40 min. Asterisks indicate GFP-positive cells. The pseudocolor scale is shown. Bar, 40 μm.

(D) Quantitative analysis of TMRM fluorescence changes over mitochondrial regions. When indicated (arrows), 1 mM H₂O₂, and 2 μM FCCP were added. Data represent average ± SEM of eight independent experiments performed as in (C).

turned to cells doubly deficient for *Mfn1* and *Mfn2* (DMF), where fusion is completely blocked (Chen et al., 2005). DMF cells appeared as sensitive to staurosporine and H₂O₂ as wt and single *Mfn1*⁻/⁻ cells, and OPA1 was effective in protecting them from apoptosis (Figures 3D and 3E). We confirmed that OPA1 inhibited release of cytochrome c in *Mfn1*⁻/⁻ and in DMF cells induced by H₂O₂ (Figures 3F and 3G) or by staurosporine (Figures S1C and S1D). Of note, *Mfn1*⁻/⁻ and DMF mitochondria expressing OPA1 remained completely fragmented, yet they retained cytochrome c, further dissociating blockage of cytochrome c release from mitochondrial fusion. Thus, OPA1 protects from apoptosis in the absence of MFN1 and MFN2. The profusion activity of OPA1 is therefore not necessary for its antiapoptotic activity.

OPA1 Controls Cytochrome c Mobilization from Mitochondrial Cristae

We verified whether OPA1 influenced the release of cytochrome c in an in vitro quantitative assay using purified organelles and recombinant proteins. Cytochrome c release from mitochondria isolated from control MEF clones carrying an empty vector with a Puromycin resistance gene (wt::*Puro* and *Mfn1*⁻/⁻::*Puro*) in response to recombinant, caspase-8-cleaved p7/p15 BID (cBID) was almost complete after 15 min. We generated clones expressing high levels of OPA1 (wt::*Opa1* and *Mfn1*⁻/⁻::*Opa1*) as confirmed by immunoblotting (Figure S2). Mitochondria isolated from these cells conversely retained a significant fraction of cytochrome c even after 15 min (Figures 4A–4D). Release was extremely fast in mitochondria isolated
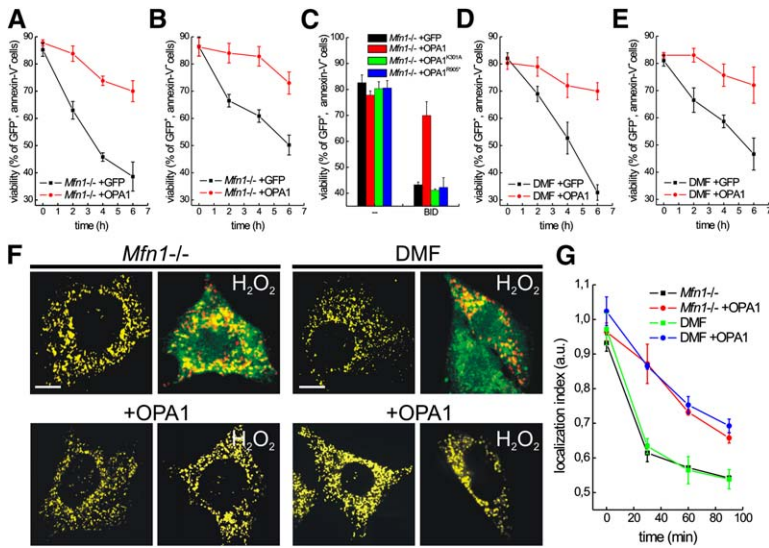
Figure 3. Mitofusins Are Not Required for the Antiapoptotic Effect of OPA1

(A–E) Cells of the indicated genotype were co-transfected with GFP and the indicated plasmids and treated with 1 mM H_2O_2 (A and D) or 2 μM staurosporine (B and E). At the indicated times, cells were harvested and viability was determined. In (C), $Mfn1^{-/-}$ MEFs were cotransfected with GFP and pcDNA3.1 or pcDNA3.1-tBID and after 24 hr viability was determined. Data represent average ± SEM of ten independent experiments.

(F) Representative images of subcellular cytochrome c distribution. Cells of the indicated genotype cotransfected with mtRFP (red) and the indicated plasmid were left untreated or treated for 30 min with 1 mM H_2O_2, fixed, and immunostained for cytochrome c (green). Bar, 10 μm.

(G) Localization index of cytochrome c. Experiments were performed as in (F), except that cells were fixed at the indicated times. Data represent average ± SEM of five independent experiments.

from MEFs expressing high levels of $OPA1^{K301A}$ (wt:: $Opa1^{K301A}$) or a short hairpin RNA interference targeting OPA1 (wt::shOpa1) (Figure S2), reaching ~85% of the total pool of cytochrome c after only 5 min (Figures 4B and 4C). Thus, levels of active OPA1 regulate the release of cytochrome c from mitochondria. The final step of cytochrome c release from mitochondria requires activation and oligomerization of the multidomain proapoptotic BCL-2 family members BAX and BAK. We found that OPA1 did not delay activation and translocation of BAX to mitochondria in

response to staurosporine (Figure S1A). Furthermore, BAK activation, measured by its oligomerization in purified mitochondria upon BID stimulation, was also unaltered (Figures 4F and 4G). Thus, OPA1 does not interfere with activation of proapoptotic members of the BCL-2 family, crucial for the permeabilization of the OM.

A small fraction of cytochrome c, corresponding to ~15%–20% of the total, is found free in the IMS, while most is located in the cristae (Scorrano et al., 2002). The OM of mitochondria can be selectively permeabilized
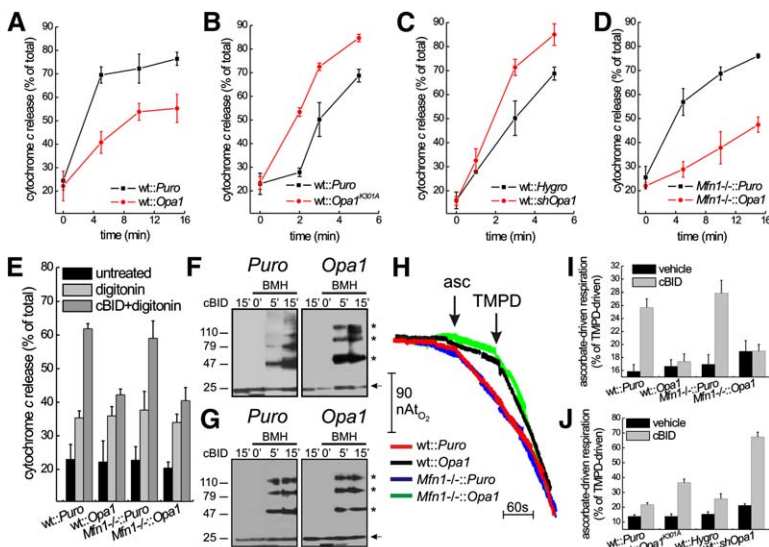
Figure 4. OPA1 Controls Mobilization of Cytochrome c from Mitochondrial Cristae in Response to BID

(A–D) Mitochondria isolated from MEFs of the indicated genotype were treated for the indicated times with cBID. After centrifugation the amount of cytochrome c in supernatant and pellet was determined by a specific ELISA. Data represent average ± SEM of four independent experiments.

(E) Mitochondria isolated from MEFs of the indicated genotype were incubated with cBID for 3 min. The OM was then permeabilized with 40 pmol digitonin × mg^{-1} mitochondria for 5 min. After centrifugation, cytochrome c content in supernatant and pellet was measured as in (A). (F and G) wt (F) and $Mfn1^{-/-}$ (G) mitochondria of the indicated genotype were treated with cBID for the indicated times. DMSO or 10 mM BMH was then added and after 30 min the crosslinking reaction was quenched (Wei et al., 2000). Equal amounts (40 μg) of mitochondrial proteins were analyzed by SDS-PAGE/immunoblotting using anti-BAK antibody. Asterisks: BAK multimers.

(H) Representative traces of ascorbate-driven respiration following BID treatment. Mitochondria of the indicated genotype were treated for 5 min with cBID and then transferred into an oxygen electrode chamber. Where indicated (arrows), 6 mM ascorbate-Tris and 300 μM TMPD were added.

(I and J) Quantitative analysis of the effect of OPA1 levels and function on BID-induced cytochrome c mobilization. Mitochondria of the indicated genotype were treated with cBID for 5 (I) or 3 min (J), and cytochrome c in the supernatant was assayed as in (D). Data represent average ± SEM of five independent experiments.
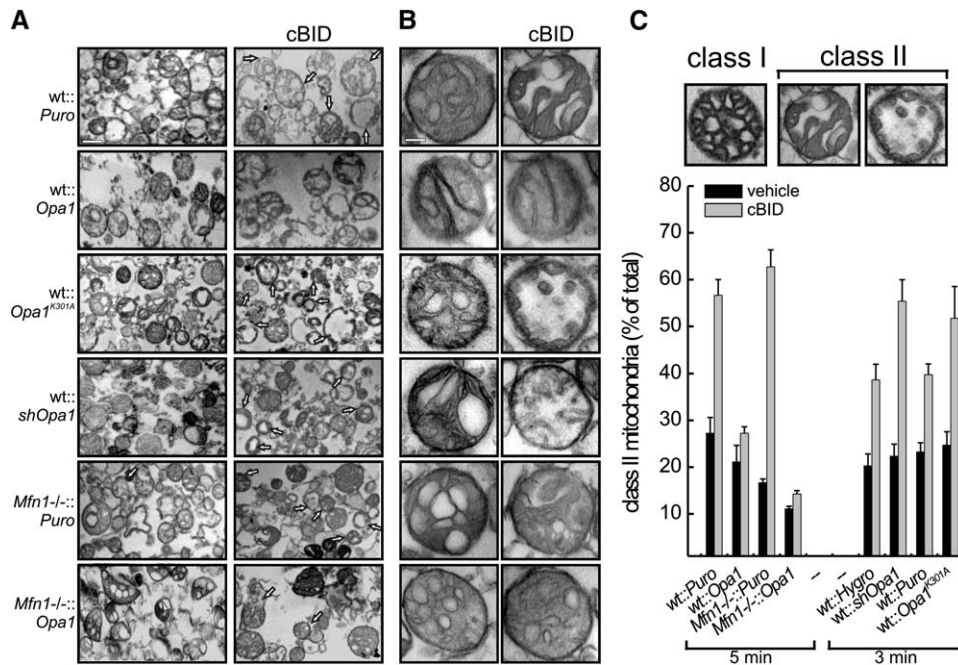
Figure 5. Mitochondrial Morphological Changes in Response to BID: Regulation by OPA1

(A) Representative EM fields of mitochondria of the indicated genotype. Where indicated, mitochondria were treated for 5 min with cBID, except for wt::*shOpa1* and wt::*Opa1*^{K301A} mitochondria, which were treated for 3 min. Arrows indicate class II mitochondria. Bar, 600 nm.

(B) Magnifications of representative transmission EM of mitochondria. Experiments were performed as in (A). Bar, 200 nm.

(C) Blind morphometric analysis of randomly selected EM fields of mitochondria of the indicated genotype. The experiments were performed as in (A). Inset shows representative class I and class II (remodeled) morphologies (Scorrano et al., 2002). Data represent average ± SEM of three independent experiments.

using titrated amounts of digitonin to selectively release the IMS pool of cytochrome c (Scorrano et al., 2002). Approximately 15% of total cytochrome c was released upon permeabilization of the outer membrane in wt and $Mfn1^{-/-}$ mitochondria, irrespective of OPA1. When wt and $Mfn1^{-/-}$ mitochondria were pretreated with cBID for 3 min, ~60% of total cytochrome c was recovered in the supernatant, confirming that at this early timepoint cBID promotes mobilization of cytochrome c from cristae to the IMS (Scorrano et al., 2002). This increase in digitonin-releasable cytochrome c upon cBID treatment was not observed in mitochondria from cells expressing OPA1 (Figure 4E). Thus, OPA1 appears to selectively stabilize the pool of cytochrome c that cBID mobilizes towards the IMS.

We therefore measured cytochrome c mobilization from cristae using a specific assay. Given the different redox potential and accessibility of membrane bound and free cytochrome c, these two pools can be specifically reduced by ascorbate and N,N,N′,N′-tetramethyl-p-phenylenediamine (TMPD) (Scorrano et al., 2002; Nicholls et al., 1980). The ratio of ascorbate over TMPD-driven O$_2$ consumption (asc/TMPD) therefore provides an estimate of the pool of free cytochrome c in the IMS relative to the total mitochondrial cytochrome c. An increase in asc/TMPD ratio reflects the mobilization of cytochrome c from the cristae stores towards the IMS (Scorrano et al., 2002).

cBID almost doubled this ratio in wt and $Mfn1^{-/-}$ mitochondria (Figures 4H and 4I). OPA1 did not affect basal asc/TMPD ratio, but it blocked the increase in the ratio observed upon cBID treatment in wt and $Mfn1^{-/-}$ mitochondria (Figures 4H and 4I). Conversely, OPA1^{K301A} and downregulation of OPA1 levels augmented the effect of cBID on the asc/TMPD ratio (Figure 4J). Of note, lower OPA1 levels resulted in a small but significant increase in basal asc/TMPD ratio (Figure 4J, p < 0.05 compared to control wt::*Hygro* mitochondria). Thus, OPA1 regulates apoptotic redistribution of cytochrome c from the cristae.

OPA1 Controls Apoptotic Remodeling of Mitochondrial Cristae

The changes in mitochondrial ultrastructure defined as "cristae remodeling" correlate with redistribution of cytochrome c from the cristae (Scorrano et al., 2002). Using conventional transmission electron microscopy (TEM), it is possible to identify remodeled "class II" mitochondria and normal "class I" mitochondria based on the appearance of the electron transparent cristae (see Figure 5C for representative images). We therefore turned to TEM of mitochondria isolated from the generated cellular models to investigate whether OPA1 influenced remodeling of the cristae. OPA1 promoted juxtaposition of the cristae membranes, generating extremely narrow structures not seen in control mitochondria (Figures 5A and 5B).

In contrast, cristae appeared wider and in wt::*Opa1*^{K301A} and wt::*shOpa1* mitochondria (Figures 5A and 5B). *Mfn1*$^{-/-}$::*Puro* and *Mfn1*$^{-/-}$::*Opa1* mitochondria displayed hyperconvex, balloon-like cristae, connected by narrow, tubular, elongated junctions to the intermembrane space (Figures 5A and 5B). cBID induced the appearance of several class II organelles in control populations (arrows in Figure 5A; magnification in Figure 5B). These remodeled mitochondria were predominant in wt::*Opa1*^{K301A} or wt::*shOpa1* as soon as 3 min after cBID (arrows in Figure 5A; magnification in Figure 5B). On the other hand, cristae of wt::*Opa1* and *Mfn1*$^{-/-}$::*Opa1* mitochondria remained narrow, and mainly class I mitochondria were retrieved following cBID (Figure 5A; magnification in Figure 5B). These observations were further corroborated by a morphometric analysis (Figure 5C).

The effect of OPA1 on mitochondrial morphology and remodeling warranted a more detailed structural investigation by electron tomography. Cristae of wt::*Puro* mitochondria appeared as pleomorphic individual structures connected to the IMS by a narrow tubular junction of 16.2 ± 2.1 nm (n = 9 in two different tomograms). wt OPA1 promoted close juxtaposition of the cristae membranes, and some cristae spanned the diameter of the reconstructed mitochondrion. The cristae junction was extremely narrow, measuring 15.2 ± 2.3 nm (n = 9 in two different tomograms) (Figure 6A). Conversely, wt::*Opa1*^{K301A} and wt::*shOpa1* cristae protruded in the matrix for less than the radius of the organelle. The narrow tubular junction was unaltered in wt::*Opa1*^{K301A} (17.1 ± 2.1 nm, n = 9 in two different tomograms) and in wt::*shOpa1* mitochondria (20.2 ± 1.6 nm, n = 9 in two different tomograms) (Figure 6A).

In wt::*Puro* mitochondria cBID promoted fusion of cristae in few intercommunicating compartments and widened the cristae junctions (45.4 ± 3.2 nm, n = 9 in two different tomograms). In wt::*Opa1* mitochondria, in contrast, cristae fused following cBID, but they retained an extremely narrow aspect, and the diameter of the tubular junction remained small (20.2 ± 3.1 nm, n = 9 in two different tomograms). Cristae junction diameter increased extremely in wt::*Opa1*^{K301A} mitochondria (65.3 ± 4.2 nm, n = 9 in two different tomograms) and in wt::*shOpa1* (73.3 ± 2.1 nm, n = 9 in two different tomograms) (Figure 6A). Rotation of a volume-rendered 3D reconstruction where the outer membrane had been peeled out allowed clear visualization of the cristae junctions (Figure 6B). In untreated mitochondria, these narrow structures were unaffected by expression of OPA1. Following cBID they became greatly enlarged, and this enlargement was entirely prevented by OPA1 expression (Figure 6B). To investigate whether OPA1 required *Mfn1* to control shape and remodeling of the cristae, we turned to *Mfn1*$^{-/-}$ mitochondria. *Mfn1*$^{-/-}$::*Puro* mitochondria showed balloon-like, hyperconvex, individual cristae coexisting with more conventional pleomorphic ones. Independently from their shape, cristae had narrow junctions of 19.0 ± 2.1 nm (n = 9 in two different tomograms).

Mfn1$^{-/-}$::*Opa1* mitochondria showed balloon cristae with some aspects of close juxtaposition of cristae membranes similar to those observed in wt::*Opa1* organelles. The narrow tubular junction of these cristae measured 18.3 ± 2.2 nm (n = 9 in two different tomograms). cBID caused fusion of *Mfn1*$^{-/-}$::*Puro* cristae and widening of their tubular junctions (41.4 ± 2.2 nm, n = 9 in two different tomograms). Conversely, junctions remained tight in *Mfn1*$^{-/-}$::*Opa1* cristae, their diameter measuring 18.5 ± 2.0 nm (n = 9 in two different tomograms) (Figure 6A). Thus, OPA1 counteracts the widening of the tubular junctions induced by cBID independently of MFN1.

Oligomers of Soluble and Membrane Bound OPA1 Are Disrupted by BID Early during Apoptosis

We turned to a biochemical approach to determine how OPA1 could control cristae shape. OPA1 is synthesized as an integral IM protein from one single gene. Alternative splicing generates eight different transcripts, all of them containing the transmembrane domain (Delettre et al., 2001), but a minor fraction of OPA1 is released in the IMS in a process that is regulated by the IM rhomboid protease PARL (Cipolat et al, 2006). The IMS form is crucial for OPA1 antiapoptotic activity (Cipolat et al., 2006). We verified whether expression of OPA1 in wt and *Mfn1*$^{-/-}$ cells resulted in an increase in IMS OPA1. Immunoblotting of membrane (pellet) and IMS (supernatant) fractions generated by hypotonic swelling and salt washes of mitochondria revealed that following expression, levels of IMS OPA1 were increased (Figure 7A). OPA1 in the membrane-enriched fraction was resistant to carbonate extraction, further indicating that this OPA1 form is integrally inserted in the IM (not shown). Consistent with this, only a minor fraction of OPA1 was released from mitochondria treated with cBID, even when cytochrome c release was complete (Figure S3). Thus, complete release of OPA1 does not occur in isolated mitochondria upon cBID treatment and can therefore not explain cristae remodeling, as previously suggested (Arnoult et al., 2005).

We therefore analyzed in greater detail OPA1 in normal and apoptotic mitochondria. Percoll-purified normal and cBID-treated, CHAPS-solubilized mouse liver mitochondria displayed very similar elution patterns from Superose 6 columns (not shown) (Danial et al., 2003). Fractions were pooled according to their size exclusion properties, designated B to E4 in descending order of molecular weight, and analyzed by SDS-PAGE and immunoblot. OPA1 was revealed in the high-molecular-weight fractions B to E2, indicating that OPA1 was part of a multimolecular complex. The matrix protein cyclophilin D used as a control was found only in fractions E3 and E4. Another OPA1 immunoreactive band with a MW corresponding to that of the soluble IMS form (Figure 7A) was found in fractions E2 ($\sim$180–230 kDa), E1 ($\sim$230–440 kDa), and D ($\sim$440–670 kDa), indicating that IMS OPA1 is also part of a multiprotein complex (Figure 7B). Following cBID, OPA1 was retrieved in fractions D, E2, and E3. p15 fragment of BID was specifically enriched in this last fraction and to a lower extent in
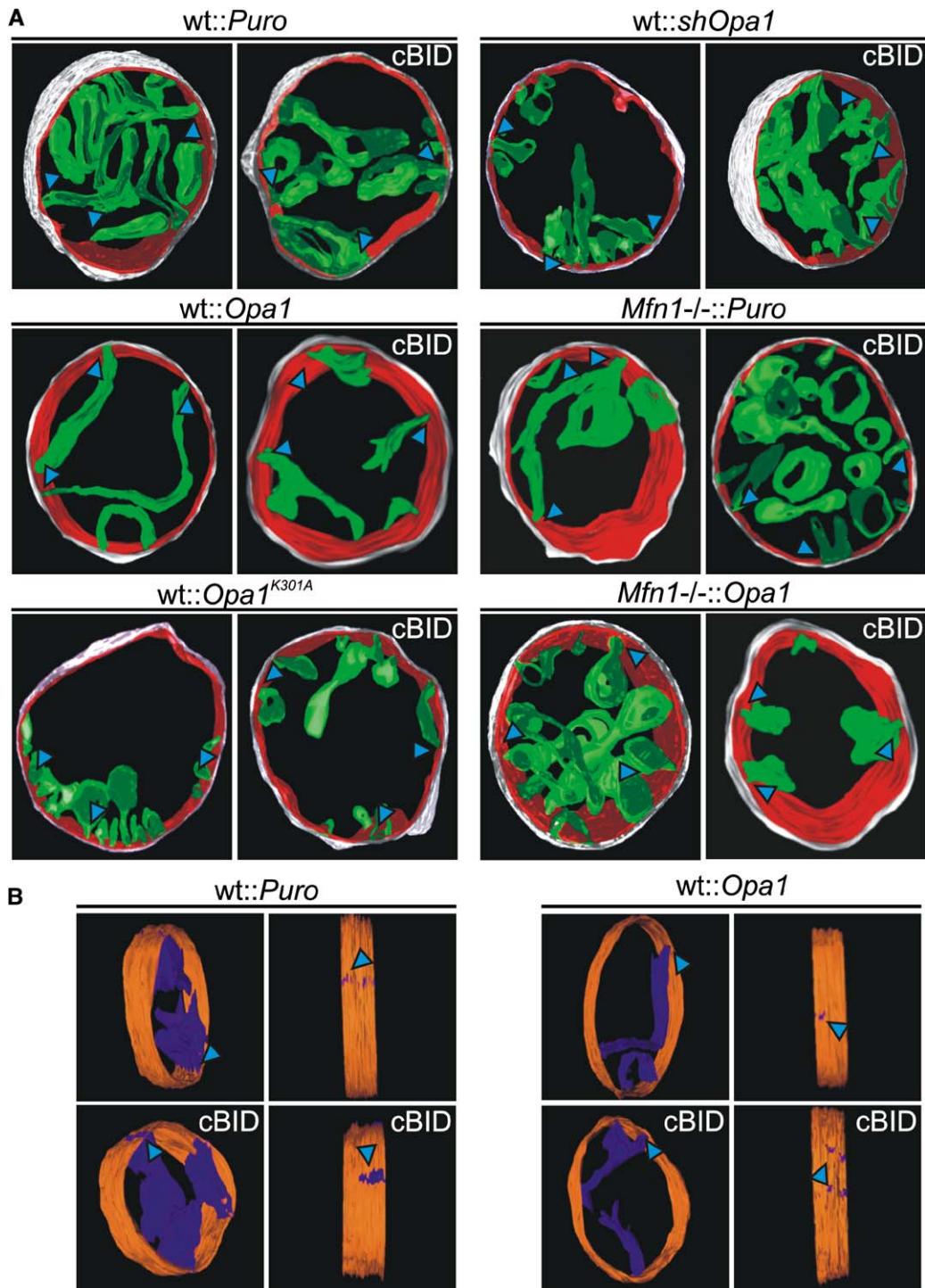
Figure 6. Electron Tomography of Mitochondrial Morphological Changes in Response to BID: Regulation by OPA1

(A) Surface-rendered views of tomographic reconstructions of mitochondria of the indicated genotype. Where indicated, mitochondria were treated with cBID for 5 min before fixation. wt::*shOpa1* and wt::*Opa1*^{K301A} mitochondria were treated for 3 min. Outer membrane is depicted in light gray, inner boundary membrane in red, and cristae in green. Cyan arrowheads point to cristae junctions. Note that selected, representative cristae were traced when their degree of interconnectivity allowed it.

(B) Rotations of representative surface rendered views of tomographic reconstructions of mitochondria. Experiment was as in (A). Cristae are depicted in purple and inner boundary membrane in orange. Outer membrane has been peeled out to highlight individual openings of the cristae junctions (arrowheads).
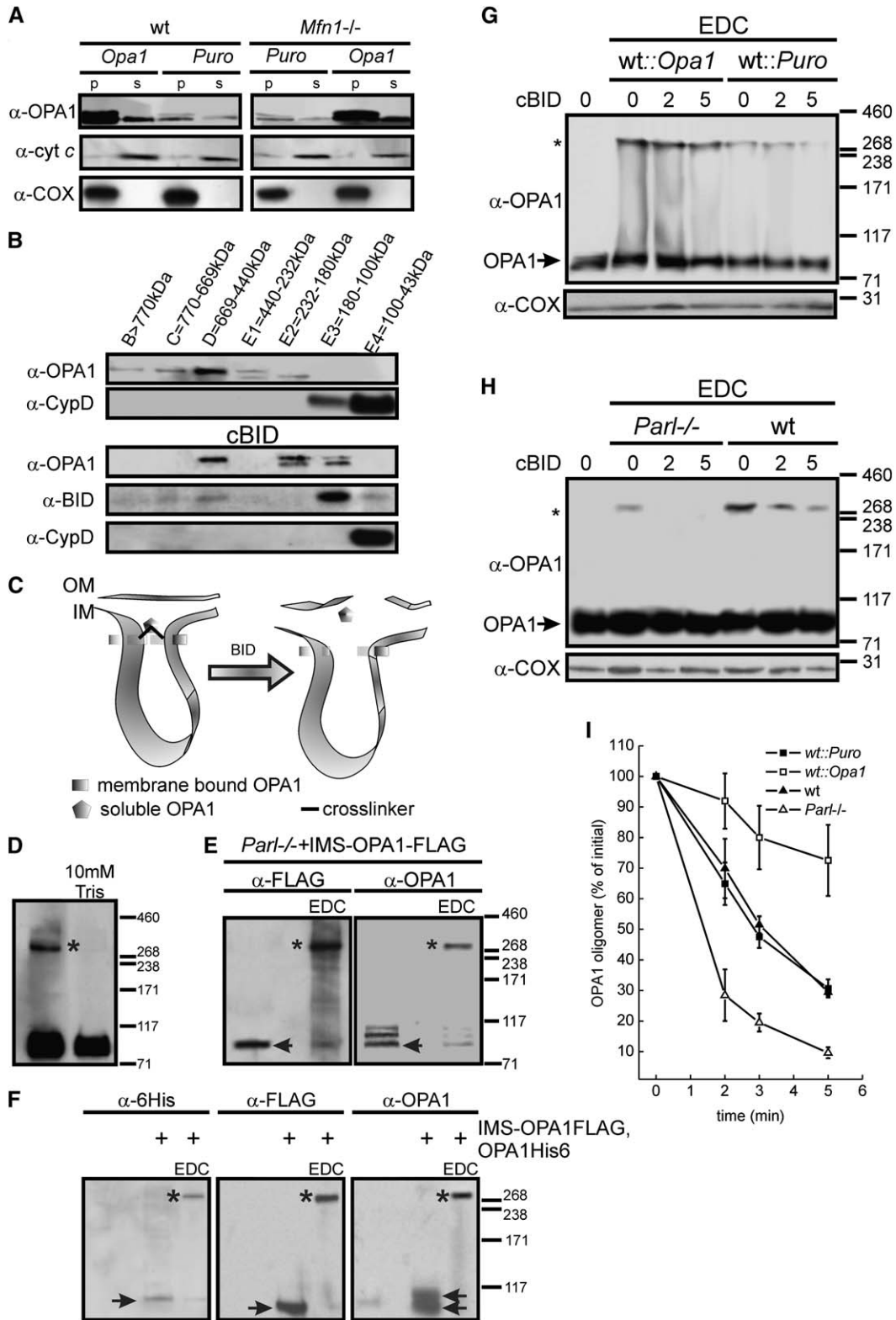
Figure 7. Oligomers Comprising IMS and Transmembrane OPA1 Are Early Targets of BID

(A) Mitochondria of the indicated genotype were hypotonically swollen and membrane (p) and soluble (intermembrane space, s) fractions were recovered. Proteins were separated by SDS-PAGE and immunoblotted with the indicated antibodies. COX indicates cytochrome c oxidase III.

fractions D, C, and E4. The matrix protein cyclophilin D was selectively enriched in low MW fraction E4 (Figure 7B). Thus, OPA1 is mainly found in high MW complexes; the lower MW form of OPA1, corresponding to IMS OPA1, is specifically enriched in fractions D to E2; and OPA1 is mainly found in lower MW fractions in apoptotic mitochondria, corresponding to smaller protein complexes.

Dynamin-related proteins are known to homo-hetero oligomerize (Danino and Hinshaw, 2001). We asked whether OPA1 could also form oligomers containing IMS and/or transmembrane forms. Such a structure could represent a molecular staple that juxtaposes the cristae membranes and could participate in the formation of the narrow tubular junction (Figure 7C). We tested whether chemical crosslinking revealed higher-order complexes immunoreactive for OPA1. A complex of OPA1 of ∼290 kDa was indeed identified in mitochondria treated with the zero-length crosslinker 1-ethyl-3-(3-dimethylamino-propyl)carbodiimide (EDC) (Figure 7D). Identical results were observed with the 16 Å crosslinker bismaleimidohexane (not shown). This complex was absent in mitochondria whose cristae had been mechanically distended by osmotic swelling (asterisk in Figure 7D). Thus, OPA1 can be crosslinked into a high-order complex only when cristae are intact. In order to understand the composition of this complex, we turned to $Parl^{-/-}$ mitochondria where IMS OPA1 is greatly reduced (Cipolat et al., 2006). Levels of OPA1 complex were also reduced, suggesting a role for IMS OPA1 in its formation (Figure 7H). A FLAG-tagged version of OPA1 selectively targeted to the IMS (IMS-OPA1-FLAG) (Otera et al., 2005; Cipolat et al., 2006) expressed in $Parl^{-/-}$ mitochondria was retrieved in the EDC-cross-linked complex by specific anti-FLAG immunoblotting (asterisk in Figure 7E). Reprobing of the membrane with an anti-OPA1 antibody revealed that IMS-OPA1-FLAG displayed an apparent MW of ∼88 kDa (arrowhead in Figure 7E), while endogenous OPA1 run at ∼100 kDa. Following crosslinking, levels of 100 kDa endogenous and of 88 kDa IMS-OPA1-FLAG were decreased, while the levels of the larger complex increased, suggesting that both IMS and transmembrane forms of OPA1 constitute

an oligomer. We further tested this by coexpressing a His-tagged version of OPA1 (OPA1-6His) with IMS-OPA1-FLAG in $Parl^{-/-}$ MEFs. As expected, ∼98% of OPA1-6His remained transmembrane in mitochondria lacking PARL, as judged by immunoblotting of membrane and IMS fractions (not shown). Transmembrane OPA1-6His and IMS OPA1-FLAG were both found in the oligomer by specific immunoblotting (Figure 7F). Thus, the oligomer contains both transmembrane and IMS OPA1.

We next assessed the fate of this OPA1 oligomer during apoptosis. The oligomer rapidly disappeared following cBID, becoming almost undetectable after 5 min (Figures 7G and 7H). Expression of OPA1 augmented levels of this oligomer and, more importantly, stabilized it in cBID-treated mitochondria (Figure 7G). In $Parl^{-/-}$ mitochondria with greatly reduced IMS-OPA1 (Cipolat et al., 2006), OPA1 oligomer was weakly represented and early disrupted by cBID (Figure 7H). A quantitative, densitometric analysis confirmed faster disappearance of the oligomer in $Parl^{-/-}$ mitochondria and its stabilization following expression of OPA1 in wt organelles (Figure 7I). Of note, destabilization of OPA1 oligomer is an initial event following cBID, occurring before the complete release of cytochrome c. In as early as 5 min, levels in the oligomer are reduced by ∼70%. This almost complete destabilization correlates with the release of approximately 80% of the cytochrome c observed at the same timepoint (Figure 4A). OPA1 oligomer is therefore an early target during cytochrome c release induced by BID. Expression of IMS-OPA1-FLAG protected $Parl^{-/-}$ MEFs from apoptosis (Cipolat et al., 2006) and prevented the enhanced cristae remodeling observed in response to cBID (Figure S4), substantiating the role of OPA1 oligomerization in this pathway.

DISCUSSION

The initial assumption that mitochondrial structure is not affected during apoptosis has been challenged during the last years. Mitochondrial fragmentation (Frank et al., 2001; Jagasia et al., 2005) and cristae remodeling (Scorrano et al., 2002; Germain et al., 2005) augment

(B) Mouse liver mitochondria were treated when indicated with cBID for 10 min, solubilized in 6 mM CHAPS, and subjected to gel filtration on Superose 6, and fractions were collected according to the indicated size exclusion properties, pooled, and concentrated. Fifty micrograms of proteins from the indicated fractions were separated by SDS-PAGE and immunoblotted with the indicated antibodies. CypD indicates cyclophilin D.

(C) Cartoon depicting the effect of BID-induced cristae remodeling on putative OPA1 oligomers; OM and IM indicate outer and inner mitochondrial membrane.

(D) Mitochondria left untreated or osmotically swollen for 10 min were incubated with 10 mM EDC for 30 min followed by centrifugation. Proteins in the pellets were separated by SDS-PAGE and immunoblotted using anti-OPA1 antibodies; the asterisk indicates OPA1 oligomer.

(E) Mitochondria were isolated from $Parl^{-/-}$ MEFs transfected with IMS-OPA1-FLAG and treated with the crosslinker EDC as in (D). Proteins were separated by SDS-PAGE and immunoblotted using the indicated antibodies; arrows indicate IMS-OPA1-FLAG, while asterisks denote OPA1 oligomer.

(F) $Parl^{-/-}$ MEFs were cotransfected with GFP and where indicated with IMS-OPA1-FLAG and OPA1-6His, sorted, and mitochondria were isolated. Where indicated, mitochondria were treated with EDC as in (D). Equal amounts of protein were separated by SDS-PAGE and immunoblotted using the indicated antibodies. Arrows indicate IMS-OPA1-FLAG and OPA1-6His, while asterisks denote OPA1 oligomer.

(G and H) Mitochondria of the indicated genotype were treated with cBID for the indicated times and then crosslinked with EDC as in (D). Proteins were separated by SDS−PAGE and immunoblotted using the indicated antibodies. Asterisk denotes OPA1 oligomer. Arrow indicates nonoligomerized OPA1. COX is cytochrome c oxidase III.

(I) Kinetics of OPA1 oligomer destabilization by cBID. OPA1 oligomer was analyzed by densitometry on Immunoblots following normalization for loading based on levels of COX. Data were normalized to levels of OPA1 oligomer in untreated mitochondria and represent average ± SEM of five independent experiments.

cytochrome c release and complete the program of mitochondrial dysfunction (Green and Kroemer, 2004). Little is known about the molecular mechanisms behind this remodeling process, but a likely candidate protein is OPA1, a dynamin-related protein of the IM, which mediates fusion of the organelle. We demonstrate here that mitochondrial remodeling and cytochrome c mobilization are regulated by levels of functional OPA1 and that this occurs independently from mitochondrial fusion. We also show that IMS and transmembrane OPA1 form oligomers that are early targets of BID during cristae remodeling.

OPA1 reduces cytochrome c release, mitochondrial dysfunction, and cell death induced by intrinsic stimuli without interfering with activation of the mitochondrial gatekeepers, the multidomain proapoptotics BAX and BAK (Scorrano and Korsmeyer, 2003). Given its function in mitochondrial fusion, one could predict that OPA1 protects by counteracting apoptotic fragmentation of mitochondria, a process observed in several paradigms of cell death (Youle and Karbowski, 2005). This appeared not to be the case since OPA1 efficiently protects cells lacking *Mfn1*, essential for OPA1-mediated mitochondrial fusion (Cipolat et al., 2004), and doubly *Mfn* null MEFs where fusion is completely abolished (Chen et al., 2005). Active OPA1 on the other hand blocks intramitochondrial cytochrome c redistribution that follows cristae remodeling (Scorrano et al., 2002; Germain et al., 2005). Previous approaches using conventional EM of mitochondria in cells with downregulated OPA1 or mgm1p (its yeast homolog) showed a gross disruption of the overall cristae morphology (Olichon et al., 2003; Amutha et al., 2004; Griparic et al., 2004). Loss of mitochondrial DNA and therefore of components of the respiratory chain contributed to this phenotype in yeast (Amutha et al., 2004). In mammalian cells, the remodeling of the cristae observed in situ can follow the activation of apoptosis caused by ablation of *Opa1* (Olichon et al., 2003). We therefore reinvestigated the role of OPA1 in biogenesis and remodeling of the cristae using tomography of mitochondria isolated from cellular models with defined levels of this protein. Electron tomography showed that OPA1 regulates shape and length of mitochondrial cristae and more importantly cristae remodeling during apoptosis. OPA1 keeps tight the cristae junction, which is likely to regulate mobilization of cytochrome c to the IMS following BID treatment. $Mfn1^{-/-}$ cristae appeared hyperconvex. Nevertheless, they were still connected by a narrow tubular junction to the IMS, and this junction widened following BID treatment. OPA1 did not change curvature of $Mfn1^{-/-}$ cristae but, significantly, blocked enlargement of the cristae junction. Thus, curvature of the cristae is not the determining factor in cytochrome c release.

How does OPA1 regulate remodeling of the cristae? One possibility is that OPA1 is released completely during apoptosis, as it has been previously reported (Arnoult et al., 2005). On the other hand, OPA1 has been found to be mainly an integral IM protein (Griparic et al., 2004; Satoh et al., 2003). We indeed observed the release of only a small pool of OPA1 corresponding to a fraction of the protein that is present in the IMS of untreated mitochondria. OPA1 exists in multiple splicing variants. Nevertheless, a transmembrane domain is present in all eight different variants and ensures integral insertion in the IM. So, how is this IMS pool of OPA1 produced? In yeast, pcp1p/rbd1p, a rhomboid protease of the IM, cleaves the transmembrane domain of mgm1p, the yeast homolog of OPA1, to generate a short form soluble in the IMS (McQuibban et al., 2003; Herlan et al., 2003). In an accompanying manuscript, evidence is provided that formation of IMS OPA1 in mammalian mitochondria appears to depend on PARL, the ortholog of rbd1p. *Parl* is also a prerequisite for the antiapoptotic function of OPA1 (Cipolat et al., 2006). This correlates with decreased levels of soluble IMS OPA1 and can be rescued by IMS OPA1 expression (Cipolat et al., 2006). We therefore investigated the potential role of IMS OPA1 at the molecular level. An indication came from studies on dynamin I, which tubulates membranes and assembles in oligomers that are crucial to sever membranes (Sweitzer and Hinshaw, 1998). OPA1 is, however, located inside the bilayer on which it should act. It therefore was unlikely that OPA1 could operate in a similar way as dynamin I. We therefore tested an alternative hypothesis in which transmembrane OPA1 uses the soluble, IMS form to oligomerize. These oligomers could "staple" the membranes of the cristae. We found support for this hypothesis in a series of experiments. First, gel filtration chromatography showed that OPA1 was found in fractions containing high MW complexes (also in HeLa mitochondria [Satoh et al., 2003]). Second, cBID destabilized these oligomers, correlating with increased cytochrome c release and apoptosis. Third, chemical crosslinking identified an ∼290 kDa OPA1 immunoreactive band that disappeared when membranes of cristae were separated by osmotic swelling. This oligomer contained the soluble IMS form and the transmembrane IM form of OPA1, as demonstrated using tagged versions of IMS and IM OPA1. Fourth, the presence and disappearance of this oligomer correlates with protection against and induction of apoptosis and cytochrome c release, respectively. Fifth, levels of IMS OPA1 are crucial for the formation of the oligomer to protect from apoptosis (Cipolat et al., 2006) and to prevent cristae remodeling. Taken together, these results suggest that OPA1 oligomers participate in formation and maintenance of the cristae junction.

The size of the OPA1 oligomer as determined by crosslinking and the retrieval of tagged versions of IMS and IM OPA1 in this oligomer suggest the hypothesis of at least a trimer comprising two IM and one IMS OPA1. However, OPA1 is also found in fractions of higher MW in both normal and apoptotic mitochondria. Thus, we cannot exclude the possibility that other proteins participate in this complex. The fact that we found OPA1 in a ∼230 to ∼180 kDa fraction following treatment with cBID would indeed suggest that OPA1 can associate with other proteins during apoptosis. This is a next challenge requiring copurification experiments and proteomic approaches in normal and apoptotic mitochondria.

Our work shows that OPA1 is a bifunctional protein. On one hand it in promotes mitochondrial fusion, depending on MFN1. On the other, it regulates apoptosis by controlling cristae remodeling and cytochrome c redistribution. This correlates with OPA1 oligomerization and is dependent on its cleavage by PARL. In conclusion, oligomerization of OPA1 appears to be a mechanism that regulates apoptosis by maintaining the tightness of cristae junctions. This unexpected role of OPA1 needs to be further explored. This mechanism could, for example, contribute to the pathogenesis of dominant optic atrophy since mutations causing this disease cluster in the GTPase and coiled-coil domains of OPA1, possibly impairing assembly and/or function of the OPA1 oligomer.

EXPERIMENTAL PROCEDURES

Cell Culture, Transfection, Sorting, and Generation of Stable Clones

SV40 transformed wt and $Mfn1^{-/-}$ MEFs were cultured as described in Cipolat et al. (2004); DMF MEFs were cultured as described in Chen et al. (2005). Cells were transfected using Transfectin (Biorad) following manufacturer's instructions.

For sorting, 1×10^8 cotransfected MEFs were analyzed by light forward and side scatter and for GFP fluorescence through a 530 nm band pass filter as they traversed the beam of an argon ion laser (488 nm, 100 mW) of an FACSAria (BD). Nontransfected MEFs were used to set the background fluorescence. Sorted cells were checked for viability by Trypan Blue exclusion.

The single clones were generated by limited dilution following transfection and antibiotic selection of expressing cells.

Analysis of Cell Death

1×10^5 MEFs of the indicated genotype grown in 12-well plates were cotransfected with pEGFP and the indicated vector. After 24 hr cells were treated as described and stained with Annexin-V-Alexa568 (Roche) according to manufacturer's protocol. Apoptosis was measured by flow cytometry (FACSCalibur) as the percentage of annexin-V-positive events in the GFP-positive population.

Transmission Electron Microscopy, Tomographic Reconstruction, and Mitochondrial Morphometry

Mitochondria were fixed for 1 hr at 25°C using glutaraldehyde at a final concentration of 2.5% (V/V). Thin sections were imaged on a Tecnai-12 electron microscope (Philips-FEI) at the Telethon EM Core Facility (TeEMCoF, Istituto Mario Negri Sud). For tomography, colloidal gold particles were applied to one side of 200 nm-thick sections as alignment markers. Tilt series of 122 images were recorded around one tilt axis, over an angular range of 120° with a 1° tilt interval. Images were aligned and reconstructed as previously described (Scorrano et al., 2002). The reconstructed volumes had dimensions of 512 × 512 × 80–100 pixels depending on section thickness, with a pixel size range of 2.5–4.1 nm. Surface-rendered models were produced using IMOD (Mironov et al., 2001) or Reconstruct (Fiala, 2005). Measurements were made directly on 1 pixel-thick tomogram slices.

Molecular Biology

p3 × FLAG-CMV14-AIF-Opa1 (IMS-OPA1-FLAG) and pCDNA3-OPA1-HA-HisTag (OPA1-6His) were kind gifts from K. Mihara (Kyushu University, Fukuoka, Japan) and P. Belenguer (U. of Toulouse, France), respectively. shRNAi were constructed to target the nucleotide region 1813–1831 of murine OPA1. All other plasmids are described in Cipolat et al. (2004).

Imaging

For cytochrome c immunolocalization, cells grown on coverslips were transfected with mtRFP and after 24 hr incubated as detailed. Immunostaining for cytochrome c was performed as described in Scorrano et al. (2003). For cytochrome c and mtRFP detection, green and red channel images were acquired simultaneously using two separate color channels on the detector assembly of a Nikon Eclipse E600 microscope equipped with a Biorad MRC-1024 laser scanning confocal imaging system. The localization index was calculated as described in Petronilli et al. (2001).

For imaging of mitochondrial membrane potential, MEFs grown on coverslips were cotransfected as indicated and after 24 hr loaded with 10 nM TMRM (Molecular Probes) in the presence of 2 μg/ml cyclosporine H, a P-glycoprotein inhibitor (30 min at 37°C). Clusters of GFP-positive cells were identified and sequential images of TMRM fluorescence were acquired every 30 s using an Olympus IMT-2 inverted microscope equipped with a CellR Imaging system.

Recombinant Proteins

p7/p15 recombinant BID was produced, purified, and cleaved with caspase-8 as described in Scorrano et al. (2002). Unless noted, it was used at a final concentration of 32 pmol × mg^{-1}.

In Vitro Mitochondrial Assays

Mitochondria were isolated by standard differential centrifugation in isolation buffer (IB). Oxygen consumption of mitochondria incubated in experimental buffer (EB) was measured using a Clarke-type oxygen electrode (Hansatech Instruments) (Scorrano et al., 2002). Cytochrome c redistribution and release in response to recombinant cBID was determined as described in Scorrano et al. (2002).

Biochemistry

For protein crosslinking, mitochondria were treated with 10 mM BMH (Pierce) or with 10 mM EDC (Pierce) for 30 min at 37°C. Samples were centrifuged for 10 min at 12000 × g at 4°C, and the mitochondrial pellets were resuspended in SDS-PAGE sample loading buffer. DTT in the sample buffer quenched the crosslinking reaction. Proteins were separated by 3%–8% Tris-Acetate or 4%–12% Tris-MES SDS-PAGE (NuPage, Invitrogen), transferred onto PVDF membranes (Millipore), and probed using the indicated primary antibodies and isotype matched secondary antibodies conjugated to horseradish peroxidase. Signals were detected using ECL (Amersham). Details on the antibodies used can be found in Supplemental Data. Densitometry was performed using a GS170 Calibrated Imaging densitometer, and data were analyzed using Quantity One software (Biorad).

For Superose 6 filtration, purified mouse liver mitochondria (50 mg) were solubilized in the presence of 6 mM CHAPS passed onto a Superose 6 column, and fractions were collected, pooled, and concentrated as described (Danial et al., 2003).

Additional details on the experimental procedures can be found in Supplemental Data available with this article online.

Supplemental Data

Supplemental Data include four figures and can be found with this article online at http://www.cell.com/cgi/content/full/126/1/177/DC1/.

REFERENCES

Adams, J.M., and Cory, S. (2001). Life-or-death decisions by the Bcl-2 protein family. Trends Biochem. Sci. *26*, 61–66.

Amutha, B., Gordon, D.M., Gu, Y., and Pain, D. (2004). A novel role of Mgm1p, a dynamin-related GTPase, in ATP synthase assembly and cristae formation/maintenance. Biochem. J. *381*, 19–23.

Arnoult, D., Grodet, A., Lee, Y.J., Estaquier, J., and Blackstone, C. (2005). Release of OPA1 during apoptosis participates in the rapid and complete release of cytochrome c and subsequent mitochondrial fragmentation. J. Biol. Chem. *280*, 35742–35750.

Chen, H., Detmer, S.A., Ewald, A.J., Griffin, E.E., Fraser, S.E., and Chan, D.C. (2003). Mitofusins Mfn1 and Mfn2 coordinately regulate mitochondrial fusion and are essential for embryonic development. J. Cell Biol. *160*, 189–200.

Chen, H., Chomyn, A., and Chan, D.C. (2005). Disruption of fusion results in mitochondrial heterogeneity and dysfunction. J. Biol. Chem. *280*, 26185–26192.

Cipolat, S., de Brito, O.M., Dal Zilio, B., and Scorrano, L. (2004). OPA1 requires mitofusin 1 to promote mitochondrial fusion. Proc. Natl. Acad. Sci. USA *101*, 15927–15932.

Cipolat, S., Rudka, T., Hartmann, D., Costa, V., Serneels, L., Craessaerts, K., Metzger, K., Frezza, C., Annaert, W., D'Adamio, L., Derks, C., Dejaegere, T., Pellegrini, L., D'Hooge, R., Scorrano, L., and De Strooper, B. (2006). Mitochondrial rhomboid PARL regulates cytochrome c release during apoptosis via OPA1-dependent cristae remodelling. Cell *126*, this issue, 163–175.

Danial, N.N., Gramm, C.F., Scorrano, L., Zhang, C.Y., Krauss, S., Ranger, A.M., Datta, S.R., Greenberg, M.E., Licklider, L.J., Lowell, B.B., et al. (2003). BAD and glucokinase reside in a mitochondrial complex that integrates glycolysis and apoptosis. Nature *424*, 952–956.

Danino, D., and Hinshaw, J.E. (2001). Dynamin family of mechanoenzymes. Curr. Opin. Cell Biol. *13*, 454–460.

Delettre, C., Griffoin, J.M., Kaplan, J., Dollfus, H., Lorenz, B., Faivre, L., Lenaers, G., Belenguer, P., and Hamel, C.P. (2001). Mutation spectrum and splicing variants in the OPA1 gene. Hum. Genet. *109*, 584–591.

Fannjiang, Y., Cheng, W.C., Lee, S.J., Qi, B., Pevsner, J., McCaffery, J.M., Hill, R.B., Basanez, G., and Hardwick, J.M. (2004). Mitochondrial fission proteins regulate programmed cell death in yeast. Genes Dev. *18*, 2785–2797.

Fiala, J.C. (2005). Reconstruct: a free editor for serial section microscopy. J. Microsc. *218*, 52–61.

Frank, S., Gaume, B., Bergmann-Leitner, E.S., Leitner, W.W., Robert, E.G., Catez, F., Smith, C.L., and Youle, R.J. (2001). The role of dynamin-related protein 1, a mediator of mitochondrial fission, in apoptosis. Dev. Cell *1*, 515–525.

Germain, M., Mathai, J.P., McBride, H.M., and Shore, G.C. (2005). Endoplasmic reticulum BIK initiates DRP1-regulated remodelling of mitochondrial cristae during apoptosis. EMBO J. *24*, 1546–1556.

Green, D.R., and Kroemer, G. (2004). The pathophysiology of mitochondrial cell death. Science *305*, 626–629.

Griparic, L., and van der Bliek, A.M. (2001). The many shapes of mitochondrial membranes. Traffic *2*, 235–244.

Griparic, L., van der Wel, N.N., Orozco, I.J., Peters, P.J., and van der Bliek, A.M. (2004). Loss of the intermembrane space protein Mgm1/

OPA1 induces swelling and localized constrictions along the lengths of mitochondria. J. Biol. Chem. *279*, 18792–18798.

Herlan, M., Vogel, F., Bornhovd, C., Neupert, W., and Reichert, A.S. (2003). Processing of Mgm1 by the rhomboid-type protease Pcp1 is required for maintenance of mitochondrial morphology and of mitochondrial DNA. J. Biol. Chem. *278*, 27781–27788.

Ishihara, N., Eura, Y., and Mihara, K. (2004). Mitofusin 1 and 2 play distinct roles in mitochondrial fusion reactions via GTPase activity. J. Cell Sci. *117*, 6535–6546.

Jagasia, R., Grote, P., Westermann, B., and Conradt, B. (2005). DRP-1-mediated mitochondrial fragmentation during EGL-1-induced cell death in C. elegans. Nature *433*, 754–760.

James, D.I., Parone, P.A., Mattenberger, Y., and Martinou, J.C. (2003). hFis1, a novel component of the mammalian mitochondrial fission machinery. J. Biol. Chem. *278*, 36373–36379.

Karbowski, M., Arnoult, D., Chen, H., Chan, D.C., Smith, C.L., and Youle, R.J. (2004). Quantitation of mitochondrial dynamics by photo-labeling of individual organelles shows that mitochondrial fusion is blocked during the Bax activation phase of apoptosis. J. Cell Biol. *164*, 493–499.

Koshiba, T., Detmer, S.A., Kaiser, J.T., Chen, H., McCaffery, J.M., and Chan, D.C. (2004). Structural basis of mitochondrial tethering by mitofusin complexes. Science *305*, 858–862.

Lee, Y.J., Jeong, S.Y., Karbowski, M., Smith, C.L., and Youle, R.J. (2004). Roles of the mammalian mitochondrial fission and fusion mediators Fis1, Drp1, and Opa1 in apoptosis. Mol. Biol. Cell *15*, 5001–5011.

Legros, F., Lombes, A., Frachon, P., and Rojo, M. (2002). Mitochondrial fusion in human cells is efficient, requires the inner membrane potential, and is mediated by mitofusins. Mol. Biol. Cell *13*, 4343–4354.

McQuibban, G.A., Saurya, S., and Freeman, M. (2003). Mitochondrial membrane remodelling regulated by a conserved rhomboid protease. Nature *423*, 537–541.

Mironov, A.A., Beznoussenko, G.V., Nicoziani, P., Martella, O., Trucco, A., Kweon, H.S., Di Giandomenico, D., Polishchuk, R.S., Fusella, A., Lupetti, P., et al. (2001). Small cargo proteins and large aggregates can traverse the Golgi by a common mechanism without leaving the lumen of cisternae. J. Cell Biol. *155*, 1225–1238.

Neuspiel, M., Zunino, R., Gangaraju, S., Rippstein, P., and McBride, H.M. (2005). Activated Mfn2 signals mitochondrial fusion, interferes with Bax activation and reduces susceptibility to radical induced depolarization. J. Biol. Chem. *26*, 25060–25070.

Nicholls, P., Hildebrandt, V., Hill, B.C., Nicholls, F., and Wrigglesworth, J.M. (1980). Pathways of cytochrome c oxidation by soluble and membrane-bound cytochrome aa3. Can. J. Biochem. *58*, 969–977.

Olichon, A., Baricault, L., Gas, N., Guillou, E., Valette, A., Belenguer, P., and Lenaers, G. (2003). Loss of OPA1 perturbates the mitochondrial inner membrane structure and integrity, leading to cytochrome c release and apoptosis. J. Biol. Chem. *278*, 7743–7746.

Otera, H., Ohsakaya, S., Nagaura, Z., Ishihara, N., and Mihara, K. (2005). Export of mitochondrial AIF in response to proapoptotic stimuli depends on processing at the intermembrane space. EMBO J. *24*, 1375–1386.

Petronilli, V., Penzo, D., Scorrano, L., Bernardi, P., and Di Lisa, F. (2001). The mitochondrial permeability transition, release of cytochrome c and cell death. Correlation with the duration of pore openings in situ. J. Biol. Chem. *276*, 12030–12034.

Santel, A., and Fuller, M.T. (2001). Control of mitochondrial morphology by a human mitofusin. J. Cell Sci. *114*, 867–874.

Santel, A., Frank, S., Gaume, B., Herrler, M., Youle, R.J., and Fuller, M.T. (2003). Mitofusin-1 protein is a generally expressed mediator of mitochondrial fusion in mammalian cells. J. Cell Sci. *116*, 2763–2774.

Satoh, M., Hamamoto, T., Seo, N., Kagawa, Y., and Endo, H. (2003). Differential sublocalization of the dynamin-related protein OPA1

isoforms in mitochondria. Biochem. Biophys. Res. Commun. *300*, 482–493.

Scaffidi, C., Fulda, S., Srinivasan, A., Friesen, C., Li, F., Tomaselli, K.J., Debatin, K.M., Krammer, P.H., and Peter, M.E. (1998). Two CD95 (APO-1/Fas) signaling pathways. EMBO J. *17*, 1675–1687.

Scorrano, L., and Korsmeyer, S.J. (2003). Mechanisms of cytochrome c release by proapoptotic BCL-2 family members. Biochem. Biophys. Res. Commun. *304*, 437–444.

Scorrano, L., Ashiya, M., Buttle, K., Weiler, S., Oakes, S.A., Mannella, C.A., and Korsmeyer, S.J. (2002). A distinct pathway remodels mitochondrial cristae and mobilizes cytochrome c during apoptosis. Dev. Cell *2*, 55–67.

Scorrano, L., Oakes, S.A., Opferman, J.T., Cheng, E.H., Sorcinelli, M.D., Pozzan, T., and Korsmeyer, S.J. (2003). BAX and BAK regulation of endoplasmic reticulum Ca^{2+}: a control point for apoptosis. Science *300*, 135–139.

Smirnova, E., Griparic, L., Shurland, D.L., and van der Bliek, A.M. (2001). Dynamin-related protein Drp1 is required for mitochondrial division in mammalian cells. Mol. Biol. Cell *12*, 2245–2256.

Sugioka, R., Shimizu, S., and Tsujimoto, Y. (2004). Fzo1, a protein involved in mitochondrial fusion, inhibits apoptosis. J. Biol. Chem. *279*, 52726–52734.

Sweitzer, S.M., and Hinshaw, J.E. (1998). Dynamin undergoes a GTP-dependent conformational change causing vesiculation. Cell *93*, 1021–1029.

Wang, X. (2001). The expanding role of mitochondria in apoptosis. Genes Dev. *15*, 2922–2933.

Wei, M.C., Lindsten, T., Mootha, V.K., Weiler, S., Gross, A., Ashiya, M., Thompson, C.B., and Korsmeyer, S.J. (2000). tBID, a membrane-targeted death ligand, oligomerizes BAK to release cytochrome c. Genes Dev. *14*, 2060–2071.

Wei, M.C., Zong, W.X., Cheng, E.H., Lindsten, T., Panoutsakopoulou, V., Ross, A.J., Roth, K.A., MacGregor, G.R., Thompson, C.B., and Korsmeyer, S.J. (2001). Proapoptotic BAX and BAK: a requisite gateway to mitochondrial dysfunction and death. Science *292*, 727–730.

Yoon, Y., Krueger, E.W., Oswald, B.J., and McNiven, M.A. (2003). The mitochondrial protein hFis1 regulates mitochondrial fission in mammalian cells through an interaction with the dynamin-like protein DLP1. Mol. Cell. Biol. *23*, 5409–5420.

Youle, R.J., and Karbowski, M. (2005). Mitochondrial fission in apoptosis. Nat. Rev. Mol. Cell Biol. *6*, 657–663.